ICES Journal of Marine Science, 56: 184–199. 1999
Article No. jmsc.1998.0432, available online at http://www.idealibrary.com on IDEAL

# Multi-frequency estimates of fish abundance: constraints of rather high frequencies

J. K. Horne and J. M. Jech

Horne, J. K. and Jech, J. M. 1999. Multi-frequency estimates of fish abundance: constraints of rather high frequencies. – ICES Journal of Marine Science, 56: 184–199.

Traditional scientific echosounders operate at discrete frequencies ranging from 38 to 420 kHz. We investigated the applicability and accuracy of length-based population estimates using commercially available acoustic frequencies and the inverse approach under ideal conditions. The inverse approach combines modelled and measured backscatter values to estimate the abundance of organisms in specified length classes. Reference backscatter values of individual fish were calculated using a Kirchhoff-ray mode backscatter model. Single and multi-cohort fish populations were simulated based on length-frequency samples from purse seine catches of threadfin shad (*Dorosoma petenense*) and used to calculate the total frequency-dependent volume backscatter of each population. A non-negative least squares (NNLS) algorithm was used to estimate total abundance and numbers of fish in each length class. Total abundance estimates were within <1–38% of population numbers. Within length-class estimates were inconsistent among frequency combinations and across length-class criteria. Increasing the number of frequencies does not guarantee improved accuracy of within length-class abundance estimates. Predictability of inverse simulations is non-linear when rather high frequencies are combined with non-monotonic scattering models. Accuracy of length-based abundance estimates is optimized by maximizing the amplitude range of reference backscatter measures and the number of features identified by reference scattering points.



Key words: abundance estimates, acoustic, backscatter model, inverse approach, Kirchhoff-ray mode.

Received 3 March 1998; accepted 16 November 1998.

*J. K. Horne and J. M. Jech: Cooperative Institute for Limnology and Ecosystems Research, University of Michigan, 2205 Commonwealth Blvd., Ann Arbor, MI 48105, USA. Correspondence to J. K. Horne: tel: +1 734 741 2269; fax: +1 734 741 2003; e-mail: horne@glerl.noaa.gov*

## Introduction

Harvest quotas of commercially important fish species are typically based on population assessments of commercial or research catch data. These analyses require age-, biomass-, or length-based estimates of abundance (e.g. Megrey, 1989; Sparre *et al*., 1989). Historically, net catches are used to obtain abundances, biomass, and length data but costs and labour per sample are high, and samples from any one gear type are representative of a small portion of the water column. Net-based research surveys can span the geographic range of a stock or species but catches are limited to specific locations in the survey area. Underwater acoustic technology quantifies organism abundance, biomass, and length continuously through the entire water column.

Echosounders have been used by aquatic scientists for several decades to acoustically monitor distributions and abundances of fish and zooplankton (Simmonds *et al*., 1992). During this period rapid advances in echosounder and computer technologies have increased the accuracy of acoustic size and abundance estimates when fish and zooplankton are dispersed (right side, Fig. 1). Conversions of acoustic size data to organism length and abundance estimates using traditional forward methods are constrained by frequency-dependent scattering of aquatic organisms, and by the ability of echosounders to resolve single organisms within aggregations. Many species of aquatic organism shoal or school at densities

1054–3139/99/020184+16 $30.00/0

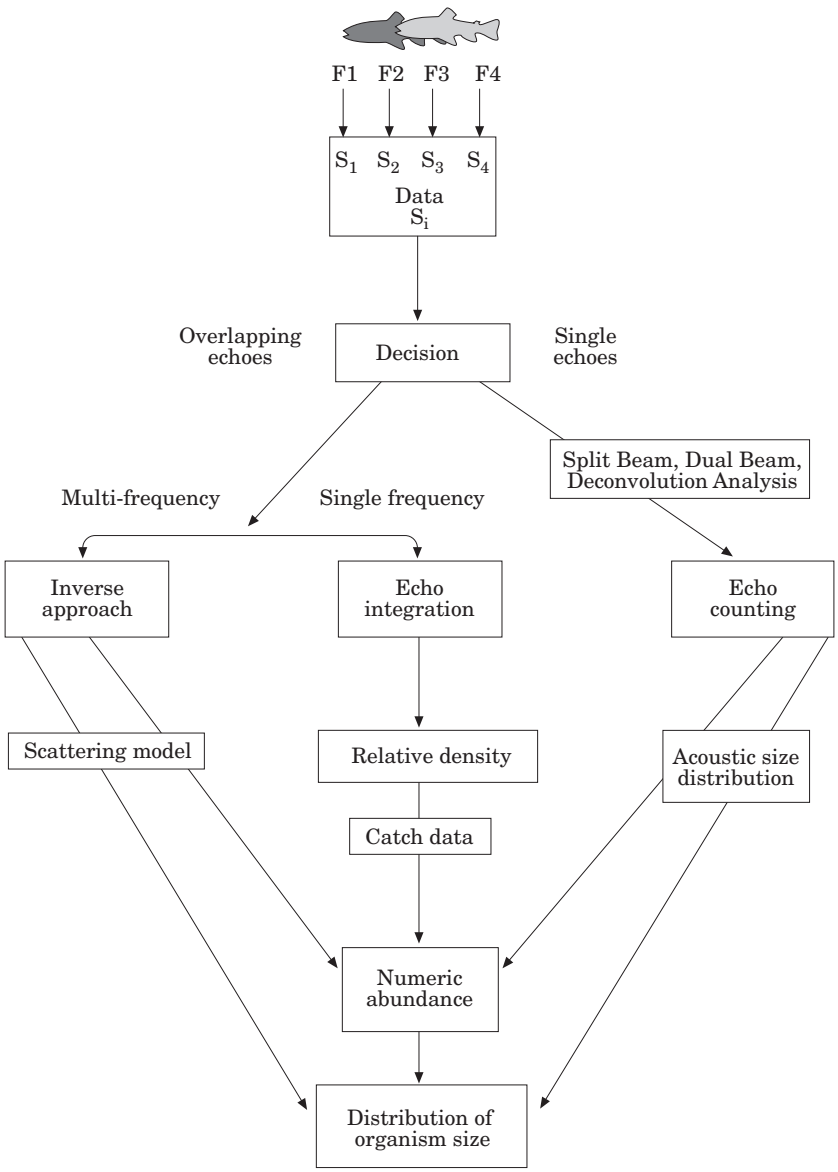


Figure 1. Schematic diagram of acoustic data processing. The right side of the diagram illustrates echo counting of single echoes. When organism packing density is high and echoes overlap, processing methods depend on the data source. If measurements were made with a single frequency (centre of diagram) then echo integration is used to estimate relative density. Supplementary data such as length-frequency abundance from net catches can be used to translate relative to numeric density. The left side of the diagram illustrates processing of overlapping echoes using the multifrequency data, the inverse approach, and theoretical backscatter models.

too high to acoustically discriminate among individuals (Dickie *et al*., 1983). Under these conditions, individuals on the periphery of an aggegation are often used to tabulate a length-frequency distribution of the group. This frequency distribution is then used in a regression equation to estimate numbers and lengths of organisms within the aggregation (e.g. Haslett, 1969; Penrose and Kaye, 1979; Williamson and Traynor, 1984). Implicit in these regression models is the assumption that the type and length-frequency distributions of organisms at the periphery matches that of individuals within the aggregation.

An alternate approach to resolving and sizing organisms within aggregations is to analyse multi-frequency acoustic data using the inverse approach. Multi-frequency acoustic data enables estimates of organism size and abundance when echoes from insonified targets overlap (McNaught, 1968, 1969; Holliday,

1977; Johnson, 1977a). The inverse approach combines backscatter model estimates of echo amplitude from individual organisms with acoustic data collected at discrete frequencies to estimate length-based abundances of insonified targets (left side, Fig. 1). Resolution of single targets is based on the frequency-dependent relationship between target size and magnitude of returned echo (Holliday, 1972, 1980). Multifrequency acoustic data and the inverse approach have been used to map length-frequency densities of small zooplankton (Holliday, 1980; Kleppel *et al.*, 1988; Holliday *et al.*, 1989; Pieper *et al.*, 1990; Smith *et al.*, 1992; Napp *et al.*, 1993), krill (Greenlaw, 1979) and small fish (Johnson, 1977b; Holliday, 1980; Kalish *et al.*, 1986), to separate fish from plankton in abundance estimates (Sætersdal *et al.*, 1984; Cochrane *et al.*, 1991), and in an attempt to classify fish by species (Zakharia and Sessarego, 1982).

Previous use of the inverse approach to estimate length-based abundances of commercial fish species is limited. This can be attributed to the traditional use of nets when sampling commercial fish populations, to the restricted availability of multi-frequency echosounders, to the lack of realistic backscatter models of fish, and to logistic constraints of using low-frequency sound sources. Greenlaw and Johnson (1983) list three critical components needed to maximize the precision of length-based abundance estimates when using the inverse approach: backscatter models that incorporate organism morphology and behaviour, accurate and precise backscatter measurements at multiple acoustic frequencies, and inversion with an accurate algorithm. Recent advances in digital echosounder technology combined with the development of anatomically-based backscatter models potentially increases the applicability of the inverse approach to estimate abundances of commercially important fish species. Holliday and Pieper (1995) stress a fourth component: that the frequencies used must span the transition from Rayleigh to geometric scattering. Backscatter measurements of fish in the Rayleigh region require sound sources operating at a few hertz to a few kilohertz. Acquiring measurements within this frequency range is logistically difficult as low frequency transducers are very large, or alternate sound sources such as explosions must be used. Low frequency data are rarely collected during standard fisheries surveys. In this paper we examine the feasibility of combining current fisheries acoustic technology with the inverse approach. The anatomically-based backscatter model of Clay and Horne (1994) is used to examine influences of geometric scattering frequency and length-class choices on abundance estimates of adult fish populations. Threadfin shad (*Dorosoma petenense*) is used as the model species in this study but the methodology is applicable to any fish species in marine or freshwater environments.

## The Inverse Approach

The premise of the inverse approach is conceptually simple. Detailed accounts can be found in Holliday (1977), Greenlaw and Johnson (1983), or Dalen and Kristensen (1990). At any frequency i, the theoretical backscatter from an ensemble of organisms $C_i$ is the sum of the backscattering cross-section of an animal $\sigma_i$ in length class j times the number of organisms n in length class j over N length classes:

$$C_i = \sum_{j=1}^{N} \sigma_{ij} n_j \tag{1}$$

To maximize the signal to noise ratio of empirical data, the number of discrete frequencies M should equal or exceed the number of length classes N. Measured volume scattering at each frequency is denoted by the vector $\mathbf{S}_i$. For example, backscatter data from a set of three frequencies divided into three length classes can be described as:

$$\begin{aligned} S_1 &= \sigma_{11} n_1 + \sigma_{12} n_2 + \sigma_{13} n_3 \\ S_2 &= \sigma_{21} n_1 + \sigma_{22} n_2 + \sigma_{23} n_3 \\ S_3 &= \sigma_{31} n_1 + \sigma_{32} n_2 + \sigma_{33} n_3 \end{aligned} \tag{2}$$

Solving this set of equations for $n_j$ provides an abundance estimate of organisms in each length class. One technique used to solve the equations for N unknowns is to minimize the sum of the squared deviations between the calculated C and measured acoustic scatter S for M frequencies:

$$\frac{\partial}{\partial n_j}\left[\sum_{i=1}^{M} (S_i - C_i)^2\right] = 0 \tag{3}$$

We used the non-negative least-squares (NNLS) algorithm from Lawson and Hanson (1974) with the constraint that negative abundances of length class are not permitted (i.e. $n_j \geq 0$ for all j). This approach can be applied to ensembles of conspecifics (e.g. Kalish *et al.*, 1986) or mixtures of species (e.g. Cochrane *et al.*, 1991).

Analysis of acoustic data using the inverse approach consists of a series of steps that are graphically portrayed in Figure 1 (left side). Acoustic data from each frequency provides the $S_i$ values. If echoes from targets overlap, then the inverse approach provides a direct estimate of organism densities. Theoretical scattering models provide values for each frequency i and each length class j. The final step uses an inverse algorithm to partition the total backscatter measured at each frequency into estimates of animal density in each length class $n_j$.

## Inverse Simulations

Theoretical scattering models of swimbladders and fish are continuously evolving (cf. Medwin and Clay, 1997; Ye *et al*., 1977; Horne and Clay, 1998). Jech *et al*. (1995) compared predictions from three backscatter models to measures of threadfin shad backscatter at 120, 200, and 420 kHz. Predictions from a Kirchhoff-ray mode (KRM) model (Clay and Horne, 1994) parameterized for shad agreed with backscatter measurements and was judged the most realistic of the three models. The KRM model represents the fish body as a set of fluid-filled cylinders surrounding a swimbladder represented by a set of gas-filled cylinders (see Appendix 1). Backscatter from the fish body and swimbladder are added coherently. Frequency-dependent, theoretical backscatter predictions in this study were calculated using a KRM model based on a digitized image of a dissected threadfin shad (Jech *et al*., 1995). In all backscatter calculations we explicitly assume that the aspect angle of all fish is zero (i.e. fish are orthogonal to the incident wave front), that fish in ensembles are randomly distributed, and that the scattering from each fish is accurately measured. Backscatter amplitude is plotted as reduced scattering length which is a non-dimensional measure of amplitude that incorporates organism length (cf. Horne and Clay, 1998).

Theoretical backscatter amplitudes of threadfin shad were calculated using the KRM model at acoustic carrier frequencies commonly used with fisheries echosounders: 38, 70, 120, 200, and 420 kHz. A reference backscatter matrix (i.e. $\sigma_{ij}$ values) was calculated at 1 mm intervals over a range of 36–112 mm total length (TL). This matrix is used in the calculation of total backscatter by ensembles of fish (i.e. the forward problem, **S**) and in estimates of the number of fish in each length class (i.e. the inverse problem, $n_j$).

Accuracy of within length class and total fish abundance estimates can not be quantified without the use of known fish populations. Two samples from purse seine catches in Lake Norman, North Carolina, USA were examined as representative populations (Schael, 1993). These samples were not normally distributed (Figs 2a and b) and mean sample lengths of 52 and 61 mm differed between the two samples ($t = -7.66$, $p<0.0001$, $df=466$). As an alternative to using catch samples, a Gaussian-random number generator was used to generate length-frequencies that represent fish populations with strong year classes. Mean and variance values used to generate fish lengths were based on length-frequency measurements from the purse seine samples. A single cohort population of 1000 shad ranged in length from 36 to 112 mm with a mean length of 75 mm and a standard deviation of 12 mm (Fig. 2c). To simulate a population with multiple cohorts, a sample of 999 lengths was compiled from three normally distributed samples with mean lengths of 50, 70, and 90 mm. Fish lengths in the trimodal population ranged from 37 to 101 mm and had a standard deviation of 16 mm (Fig. 2d).

The first step in each simulation was to choose specific acoustic carrier frequencies. The number of frequencies could range from three to five with specific frequencies grouped in any combination. For each frequency used in a simulation, the total backscatter of the population (**S** values) was calculated by summing the abundance at each fish length multiplied by the backscattering cross-section ($\sigma_{ij}$) from the KRM model at that length. The next step was to choose means and ranges of length classes for inverse calculations. In inverse calculations, all fish lengths within a length class are assumed equal to the median length. Therefore, the backscatter matrix used in any inversion consisted of $\sigma_{ij}$ values that corresponded to the median length in each length class at each frequency. Initially the number of length classes was set equal to the number of frequencies used in a data simulation (i.e. even-determined problem). To assess potential improvements in abundance estimates by increasing the number of frequencies, the same inverse simulations were repeated with more frequencies than length classes (i.e. over-determined problem). Four criteria were used to select length classes in the unimodal population: (1) equal intervals across the range of fish lengths; (2) equal intervals centred on the mean of the population; (3) intervals partitioned by the mean and one standard deviation from the mean length; and (4) intervals partitioned by the mean and two standard deviations from the mean length. These length-class criteria were selected assuming that representative length-frequency data could be obtained from net samples. All possible combinations of three, four, or five frequencies were used in even- or over-determined simulations for each length-class criterion. In simulations using the trimodal population, we used three criteria: (1) intervals centred on modal lengths; (2) intervals partitioned at the modes and nulls of the population; and (3) length classes centred at the mean $\pm$ 1,2 standard deviations. The NNLS algorithm was used to estimate the number of fish in each length class ($n_j$ values) in all simulations.

Data simulations using the inverse approach and known populations are designed to examine the influence of acoustic carrier frequency and length-class choices on length-based abundance estimates of adult fish. Accuracy of an inverse simulation was quantified using indices that measured the per capita deviance from the known population. The total population estimate index $\Delta_{total}$ measured the absolute deviance between the predicted $\hat{n}$ and known n populations:

$$\Delta_{total} = \left| \frac{\hat{n} - n}{n} \right| \tag{4}$$

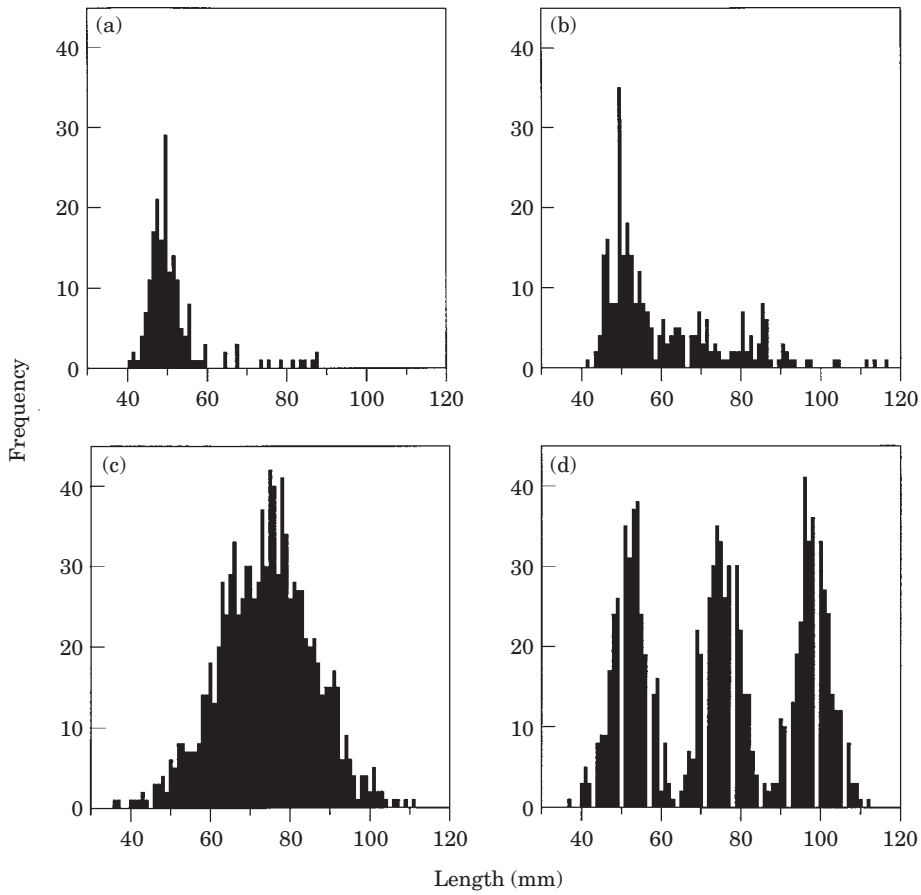


Figure 2. (a, b) Length-frequency distributions of threadfin shad (*Dorosoma petenense*) samples from purse seine catches in Lake Norman, North Carolina, USA [(a) n=183, $\bar{x}$=51.9 mm; (b) n=292, $\bar{x}$=61.2 mm]. Simulated length-frequency distributions for (c) a unimodal population (n=1000, $\bar{x}$=75) and (d) a trimodal population (n=999, $\bar{x}$=70).

The within length-class index $\Delta_{within}$ summed the absolute, proportional deviance between the predicted $\hat{n}$ and known n in each length class j:

$$\Delta_{within} = \sum_{j=1}^{N} \left| \frac{\hat{n}_j - n_j}{n} \right| \quad (5)$$

Expected values of all deviation indices are zero.

## Results

Estimates of total abundance closely approximated both uni- and trimodal population numbers. Within length-class abundance estimates were inconsistent among frequency combinations and across length-class criteria (Table 1). Among unimodal simulations, total deviation index values (mean $0.078 \pm 0.082$ s.d., n=68) were smaller than within length-class deviation index values (mean $8.32 \pm 13.6$ s.d., n=68) (Table 2). Within length-class deviation index values ranged 65 fold (1.11–65.9) in even-determined simulations. Total deviation index values were lower than within length-class index values but still ranged over three orders of magnitude (0.004–0.377). Multi-cohort index values spanned over four orders of magnitude in the within length-class deviation index (0.033–90.7) and three orders of magnitude in the total deviation index (0.002–0.127).

We identified potential "best" choices of acoustic carrier frequency and length-class combinations as simulations whose deviation index values were equal to or less than one standard error of the predicted value of 0. Within length-class and total deviation index values equal to or below one standard error of all even-determined simulations (within=1.65, total=0.01) are marked with an asterisk in Table 2. All three within length-class deviation values less than one standard error from three frequency simulations included 38, 70, and 120 kHz. When comparable within length-class estimates were calculated for over-determined solutions (i.e. four or five frequencies, three length classes), increasing the number of frequencies to four resulted in five

Table 1. Expected and observed, within length-class and total abundance estimates. Expected values are italicized. Simulations are grouped by number of length classes and number of frequencies. Multi-cohort simulations are listed in the last column.

| Length-class criterion | Equal intervals across range | | | | Equal intervals centred on mean | | | | Mean ± 1 standard deviation | | | | Mean ± 2 standard deviations | | | | Modes | | | |
|---|---|---|---|---|---|---|---|---|---|---|---|---|---|---|---|---|---|---|---|---|
| Frequency combination | Within | | Total | | Within | | Total | | Within | | Total | | Within | | Total | | Within | | Total | |
| *Expected* 3, 3 | *122* | *734* | *144* | *1000* | *135* | *739* | *126* | *1000* | *155* | *701* | *144* | *1000* | *26* | *954* | *20* | *1000* | *334* | *337* | *328* | *999* |
| 38, 70, 120 | 90 | 856 | 0 | 946 | 137 | 812 | 0 | 949 | 68 | 891 | 0 | 959 | 42 | 918 | 0 | 960 | 300 | 443 | 241 | 985 |
| 38, 70, 200 | 990 | 0 | 0 | 990 | 5 | 980 | 0 | 985 | 331 | 0 | 786 | 1117 | 49 | 934 | 0 | 983 | 317 | 404 | 268 | 989 |
| 38, 70, 420 | 302 | 158 | 618 | 1078 | 299 | 195 | 578 | 1073 | 338 | 35 | 727 | 1100 | 276 | 0 | 875 | 1151 | 347 | 333 | 317 | 997 |
| 38, 120, 200 | 0 | 959 | 0 | 959 | 0 | 966 | 0 | 966 | 0 | 941 | 27 | 968 | 0 | 966 | 0 | 966 | 311 | 430 | 245 | 986 |
| 38, 120, 420 | 426 | 529 | 0 | 955 | 407 | 556 | 0 | 963 | 444 | 499 | 0 | 943 | 0 | 676 | 239 | 916 | 380 | 340 | 275 | 995 |
| 38, 200, 420 | 191 | 78 | 828 | 1097 | 0 | 0 | 1099 | 1099 | 250 | 11 | 846 | 1107 | 0 | 370 | 730 | 1100 | 335 | 331 | 332 | 997 |
| 70, 120, 200 | 2 | 974 | 0 | 976 | 5 | 999 | 0 | 1004 | 0 | 1008 | 0 | 1008 | 0 | 883 | 153 | 1036 | 304 | 440 | 238 | 982 |
| 70, 120, 420 | 269 | 551 | 0 | 820 | 269 | 574 | 0 | 842 | 311 | 492 | 0 | 804 | 319 | 407 | 0 | 726 | 360 | 385 | 194 | 939 |
| 70, 200, 420 | 310 | 22 | 833 | 1164 | 1150 | 0 | 0 | 1150 | 954 | 0 | 0 | 954 | 167 | 0 | 1210 | 1377 | 345 | 326 | 333 | 1005 |
| 120, 200, 420 | 0 | 390 | 487 | 878 | 0 | 414 | 455 | 869 | 0 | 364 | 522 | 886 | 0 | 716 | 105 | 821 | 397 | 303 | 341 | 1042 |
| *Overdetermined* 3, 4 | | | | | | | | | | | | | | | | | | | | |
| 38, 70, 120, 200 | 10 | 954 | 0 | 964 | 21 | 952 | 0 | 974 | 24 | 951 | 0 | 975 | 17 | 959 | 0 | 976 | 307 | 433 | 245 | 985 |
| 38, 70, 120, 420 | 248 | 517 | 183 | 948 | 268 | 577 | 92 | 937 | 257 | 485 | 206 | 948 | 131 | 658 | 124 | 913 | 353 | 344 | 297 | 993 |
| 38, 70, 200, 420 | 288 | 101 | 719 | 1108 | 270 | 70 | 793 | 1133 | 1017 | 0 | 0 | 1017 | 206 | 233 | 682 | 1121 | 343 | 332 | 324 | 999 |
| 38, 120, 200, 420 | 69 | 426 | 485 | 980 | 115 | 490 | 372 | 972 | 0 | 408 | 570 | 978 | 0 | 750 | 177 | 926 | 352 | 342 | 305 | 999 |
| 70, 120, 200, 420 | 189 | 487 | 266 | 942 | 186 | 543 | 218 | 947 | 216 | 424 | 304 | 944 | 200 | 618 | 0 | 819 | 348 | 339 | 316 | 1022 |
| *Overdetermined* 3, 5 | | | | | | | | | | | | | | | | | | | | |
| 38, 70, 120, 200, 420 | 196 | 466 | 329 | 991 | 196 | 531 | 259 | 986 | 210 | 422 | 362 | 994 | 102 | 738 | 86 | 925 | | | | |
| *Expected* 4, 4 | *54* | *416* | *480* | *50* | *1000* | | | | | | | *1000* | *26* | *474* | *480* | *20* | *1000* | | | |
| 38, 70, 120, 200 | 149 | 189 | 614 | 106 | 1058 | | | | 43 | 520 | 403 | 0 | 966 | 221 | 43 | 612 | 216 | 1092 | | |
| 38, 70, 120, 420 | 0 | 0 | 0 | 1168 | 1168 | | | | 133 | 316 | 521 | 3 | 973 | 281 | 0 | 602 | 228 | 1111 | | |
| 38, 70, 200, 420 | 78 | 404 | 167 | 410 | 1059 | | | | 219 | 257 | 0 | 599 | 1074 | 0 | 0 | 218 | 1147 | 1365 | | |
| 38, 120, 200, 420 | 230 | 422 | 372 | 0 | 1024 | | | | 0 | 252 | 722 | 0 | 974 | 1023 | 0 | 0 | 3 | 1026 | | |
| 70, 120, 200, 420 | 0 | 243 | 749 | 222 | 1214 | | | | 1061 | 0 | 0 | 0 | 1061 | 244 | 0 | 653 | 273 | 1170 | | |
| *Overdetermined* 4, 5 | | | | | | | | | | | | | | | | | | | | |
| 38, 70, 120, 200, 420 | 48 | 65 | 84 | 103 | 1019 | | | | 91 | 378 | 501 | 4 | 974 | 280 | 0 | 608 | 225 | 1113 | | |
| *Expected* 5, 5 | *26* | *210* | *504* | *235* | *25* | *1000* | *31* | *238* | *498* | *209* | *24* | *1000* | | | | | *68* | *251* | *393* | *238* | *50* | *1000* |
| 38, 70, 120, 200, 420 | 75 | 154 | 373 | 338 | 83 | 1024 | 24 | 260 | 404 | 274 | 46 | 1008 | | | | | 72 | 243 | 350 | 226 | 118 | 1009 |

Table 2. Expected and observed deviation index values for within length-class† and total‡ abundance estimates. Expected values are italicized. Simulations are grouped by number of length-classes and number of frequencies. Index values within one standard error of 0 are marked with an asterisk. Multi-cohort simulations are listed in the last column.

| Length-class criterion | Equal intervals across range | | Equal intervals centred on mean | | Mean ± 1 standard deviation | | Mean ± 2 standard deviations | | Modes | |
|---|---|---|---|---|---|---|---|---|---|---|
| Frequency combination | $\Delta_{within}$ | $\Delta_{total}$ | $\Delta_{within}$ | $\Delta_{total}$ | $\Delta_{within}$ | $\Delta_{total}$ | $\Delta_{within}$ | $\Delta_{total}$ | $\Delta_{within}$ | $\Delta_{total}$ |
| *Expected* 3, 3 | *0* | *0* | *0* | *0* | *0* | *0* | *0* | *0* | *0* | *0* |
| 38, 70, 120 | 1.429* | 0.054 | 1.114* | 0.051 | 1.832 | 0.041 | 1.653 | 0.040 | 0.682* | 0.014 |
| 38, 70, 200 | 9.115 | 0.010* | 2.289 | 0.015 | 6.594 | 0.117 | 1.906 | 0.017 | 0.372* | 0.010* |
| 38, 70, 420 | 5.552 | 0.078 | 5.538 | 0.073 | 6.179 | 0.100 | 53.365 | 0.151 | 0.084* | 0.002* |
| 38, 120, 200 | 2.307 | 0.041 | 2.307 | 0.034 | 2.155 | 0.032 | 2.013 | 0.034 | 0.397* | 0.013 |
| 38, 120, 420 | 3.771 | 0.045 | 3.262 | 0.037 | 3.153 | 0.057 | 12.241 | 0.084 | 0.308* | 0.004* |
| 38, 200, 420 | 6.209 | 0.097 | 9.722 | 0.099 | 6.472 | 0.107 | 37.112 | 0.100 | 0.033* | 0.002* |
| 70, 120, 200 | 2.311 | 0.024 | 2.315 | 0.004* | 2.438 | 0.008* | 7.724 | 0.036 | 0.670* | 0.017 |
| 70, 120, 420 | 2.454 | 0.180 | 2.216 | 0.158 | 2.305 | 0.196 | 12.843 | 0.274 | 0.629* | 0.060 |
| 70, 200, 420 | 7.296 | 0.164 | 9.519 | 0.150 | 7.155 | 0.046 | 65.923 | 0.377 | 0.081* | 0.006* |
| 120, 200, 420 | 3.851 | 0.122 | 4.051 | 0.131 | 4.106 | 0.114 | 5.500 | 0.179 | 0.329* | 0.043 |
| *Overdetermined* 3, 4 | | | | | | | | | | |
| 38, 70, 120, 200 | 2.218 | 0.036 | 2.133 | 0.026 | 2.202 | 0.026 | 1.351* | 0.024 | 0.619* | 0.014 |
| 38, 70, 120, 420 | 1.560* | 0.052 | 1.474* | 0.063 | 1.397* | 0.052 | 9.549 | 0.087 | 0.172* | 0.006* |
| 38, 70, 200, 420 | 6.216 | 0.108 | 7.199 | 0.133 | 7.561 | 0.017 | 40.779 | 0.121 | 0.054* | 0* |
| 38, 120, 200, 420 | 3.222 | 0.020 | 2.437 | 0.022 | 4.376 | 0.022 | 9.064 | 0.074 | 0.139* | 0* |
| 70, 120, 200, 420 | 1.733 | 0.058 | 1.373* | 0.053 | 1.900 | 0.056 | 8.045 | 0.181 | 0.084* | 0.003* |
| *Overdetermined* 3, 5 | | | | | | | | | | |
| 38, 70, 120, 200, 420 | 2.256 | 0.009* | 1.789 | 0.014 | 2.267 | 0.006* | 6.449 | 0.075 | 0.115* | 0.001* |
| *Expected* 4, 4 | *0* | *0* | | | *0* | *0* | *0* | *0* | | |
| 38, 70, 120, 200 | 3.704 | 0.058 | | | 2.362 | 0.034 | 18.484 | 0.092 | | |
| 38, 70, 120, 420 | 25.360 | 0.168 | | | 1.669 | 0.027 | 21.462 | 0.111 | | |
| 38, 70, 200, 420 | 8.325 | 0.059 | | | 4.828 | 0.074 | 58.896 | 0.365 | | |
| 38, 120, 200, 420 | 4.499 | 0.024 | | | 3.230 | 0.026 | 41.196 | 0.026 | | |
| 70, 120, 200, 420 | 5.416 | 0.214 | | | 8.845 | 0.026 | 22.395 | 0.170 | | |
| *Overdetermined* 4, 5 | | | | | | | | | | |
| 38, 70, 120, 200, 420 | 2.538 | 0.019 | | | 1.888 | 0.026 | 21.286 | 0.887 | | |
| *Expected* 5, 5 | *0* | *0* | *0* | *0* | | | *0* | *0* | | |
| 38, 70, 120, 200, 420 | 5.170 | 0.024 | 1.735 | 0.008* | | | 1.611* | 0.009* | | |

†$\Delta_{within} = \sum_{j=1}^{N} \left| \frac{\hat{n}_j - n_j}{n_j} \right|$ where $\hat{n}$ is the predicted abundance and n is the known abundance in the j th length class. Standard error = 1.65 unimodal, 7.5 trimodal.

‡$\Delta_{total} = \left| \frac{\hat{n} - n}{n} \right|$ where $\hat{n}$ is the predicted total abundance and n is the known total abundance. Standard error = 0.01 unimodal, 0.01 trimodal.

additional frequency combinations with low deviation index values. Over-determined solutions using five frequencies and four length classes did not result in any additional within length-class deviation values less than one standard error of the mean. Among even-determined, unimodal simulations, any combination of four frequencies did not result in deviation index values less than one standard error of the expected value. Over-determined solutions for five frequencies using four length classes decreased index values but not to values less than the one standard error cutoff.

Within length-class index values less than 1.65 were found in all four length-class categories and most frequent in the equal intervals across the length range criterion (three of six cases among three length-class simulations). Total shad population abundances were underestimated in all six of the "best" three frequency simulations (Table 1). Only one of the three, five frequency within length-class index values was less than one standard error of the expected value.

Among multi-cohort simulations, 11 of 12 within length-class deviation index values were less than the standard error. Two even-determined, five frequency simulations increased the estimate of the within length-class standard error to 7.5 and due to space limitations are reported here rather than in Table 2. Using modes and nulls as length-class dividers, predicted and expected (bracketed) length-class abundances were 346 (311),

0 (73), 0 (292), 396 (73), and 308 (280). When the mean ± 1,2 standard deviations were used as length-class dividers, predicted and expected abundance estimates were 0 (66), 396 (339), 0 (314), 553 (278), and 177 (2) in the five length classes. Corresponding within length-class deviations indices were 6.637 and 90.657.

All five "best" estimates of total abundance among unimodal simulations (s.e. $\leq 0.01$) included 70 and 200 kHz (Table 1). Total abundance deviation index values were consistently low with any combination of frequency or length-class choices. Total deviation index values less than one standard error did not result from any combination of four frequencies in even- or over-determined simulations. The lowest total deviation index value among unimodal simulations resulted from a combination of 70–120–200 kHz carrier frequencies and a length-class criterion of equal intervals centred on the population mean length. Five of twelve (42%) deviation index values met the "best" total selection criterion in multi-cohort simulations (Table 2). These five simulations used three acoustic frequencies with length classes centred at the three modes of the multi-cohort population. Carrier frequencies 38 and 420 kHz were common in four of these five data simulations.

## Discussion

The goal of this project was straightforward. Given five discrete acoustic frequencies available to fisheries scientists and an anatomically-based backscatter model, can we use the inverse approach to obtain length-based estimates of fish abundance? Assuming that inverse estimates were possible, a second goal was to determine the best combination of carrier frequencies and mean fish lengths to use in inverse calculations. Early efforts using the inverse approach and multifrequency acoustic data cautioned that the accuracy of the technique was limited by the lack of validated backscatter models (e.g. Holliday, 1977; Greenlaw and Johnson, 1983). This caveat is no longer valid as an increasing number of validated models are available for both zooplankton (Stanton, 1988, 1989; Stanton *et al.*, 1993a,b) and fish (Foote, 1985; Clay and Horne, 1994; Jech *et al.*, 1995; Ye, 1997).

Despite the use of a validated backscatter model, a fundamental condition of multifrequency inverse methods could not be met in this study. Holliday and Pieper (1995) stress that the ratio of organism sizes to acoustic carrier frequencies must span the transition from Rayleigh to geometric scattering. The transition from Rayleigh to geometric scattering is a unique length-based character of the scattering curve. The KRM model predicts resonance among shad to range from 400 Hz for a 112 mm fish ($L/\lambda = 0.0298$) to 1.4 kHz for a fish 36 mm in length ($L/\lambda = 0.0336$) (Fig. 3). Commercially available echosounders rarely, if ever, bracket the transition range from Rayleigh to geometric scattering by commercial fish species. To obtain low frequency backscatter measurements for inverse calculations, Thompson and Love (1996) and Nero *et al.* (1997) found that small explosives provided the optimal sound source when estimating abundances of deep-dwelling species. The geometric scattering region includes constructive and destructive interference modes but there may be other frequency-dependent scattering amplitudes associated with length along non-monotonic scattering curves.

When fish length over acoustic wavelength ratios are constrained to the geometric scattering region, the ability to predict accuracy of inversion results using different frequency and mean length combinations is not intuitive. This lack of predictability may be considered the result of an ill-conditioned and ill-posed problem, but the exercise provided insight on the choice and interaction of three factors that influence inversion results: mean fish lengths, acoustic carrier frequencies, and backscatter models. Choice of mean fish lengths and acoustic carrier frequencies are dependent on each other. Mean fish lengths and carrier frequencies determine the range and locations of reference values on the theoretical backscatter curve. The location of a reference value depends on the ratio of mean fish length to carrier frequency wavelength (Fig. 4). All inverse simulations that fit the "best" deviation index criteria encompassed a near-maximal range of backscatter amplitudes, minimized the amount of overlap among reference scattering points, and maximized the number of features defined on the theoretical backscatter curve. We define a feature of a backscatter model as a recognizable peak or valley on the theoretical curve. Three reference values (local minimum or maximum and two inflection points) are the minimum number of points needed to denote a feature.

A judicious combination of acoustic carrier frequencies maximizes the range of scattering amplitudes used in inversion calculations. Fish lengths used in simulations ranged from 36 to 112 mm. These minimum and maximum lengths determine the proportion of the scattering curve encompassed by each frequency (Fig. 5). Since the abscissa is the ratio of fish length to acoustic wavelength, larger amounts of the scattering curve are included as carrier frequency increases. All frequency-dependent sections of the scattering curve overlap with preceding and succeeding frequency sections. To maximize the range of scattering amplitudes used in inverse calculations of shad abundance, two carrier frequencies should be chosen from two different frequency pairs: 38 or 70 kHz should be combined with 120 or 200 kHz. All 15 of the "best" within or total deviation index values from unimodel simulations contained a minimum of three of these four frequencies (Table 2).

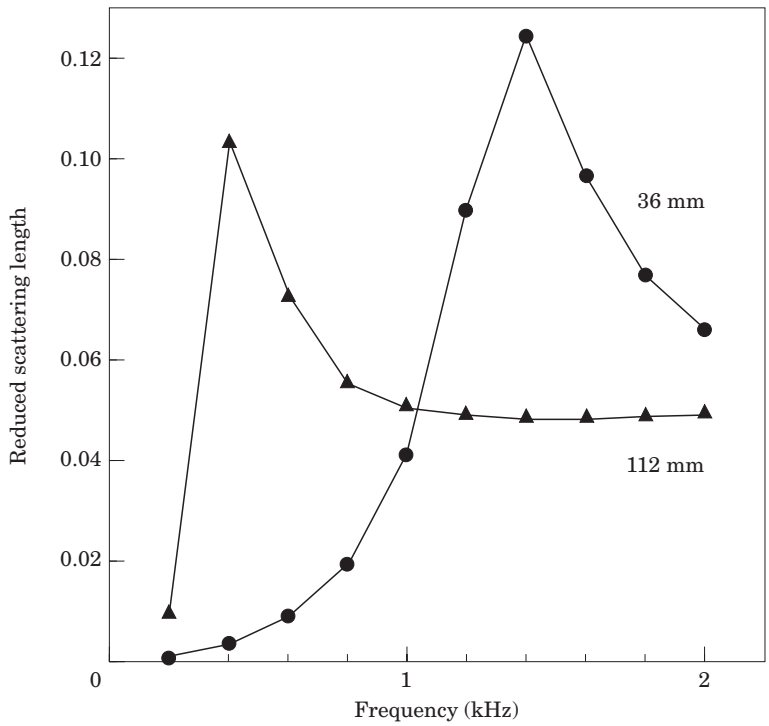


Figure 3. Kirchhoff-ray mode backscatter model predicted low-frequency scattering curves of 36 and 112 mm threadfin shad (*Dorosoma petenense*). Backscatter amplitudes peak at resonance frequencies that are well below the operating range of current fisheries echosounders (12–420 kHz).

The choice of scattering model used in the inversion will influence accuracy of population estimates. Backscatter models are either statistically derived from *in situ* measurements or are based on geometric models that incorporate organism morphology. Empirical, log-linear models typically relate echo amplitude to organism length and possibly carrier frequency or aspect (e.g. Love, 1977; Foote, 1987). Geometric (e.g. Anderson, 1950; Clay and Horne, 1994) or hybrid geometric/empirical (Dalen and Kristensen, 1990) models include resonances and interferences which result in non-monotonic scattering curves. One consequence of using non-monotonic backscatter models with single acoustic carrier frequencies is that an organism length changes, backscatter amplitudes can increase, decrease, or remain the same (Holliday and Pieper, 1995). To illustrate the potential ambiguity by example, reduced scattering lengths of threadfin shad in Fig. 4 potentially range from 0 to 0.065 as fish length increases 30-fold. The scattering curve has nine different ratio values with scattering lengths of 0.03. Similarly, changes in acoustic frequency can lead to increases or decreases in scattering amplitude for the same size organism. Models which include morphological or physical properties of the organism are preferred for inversion calculations as they can be adapted to any species, and can be interpolated to frequencies or lengths not measured (Greenlaw and Johnson, 1983).

As with any simulation exercise, initial assumptions and conditions potentially influence the accuracy of abundance estimates. We assumed that fish populations could be modelled using uni- and trimodal Gaussian distributions. The intention was to depict populations of single or multiple fish cohorts. Length-frequency distributions from sampled purse seine catches were not adequately represented by a normal distribution (Fig. 2). Length- or age-frequencies of fish populations typically contain modes and are often modelled using gamma, negative binomial, or Poisson frequency distributions. If bias was introduced through the use of normally distributed length-frequencies, this bias was constant in all inverse data simulations.

An initial condition that potentially influences inversion accuracy is the amount of "noise" in calculations of total backscatter from a population. The use of 1 mm length resolution to calculate total backscatter from simulated populations reduces the signal to noise ratio in inverse simulations. The inverse algorithm assumes that the length of each animal is equal to the median in each length class. A large range of organism sizes in any length class will increase variance in forward scattering estimates. Knowledge of the population

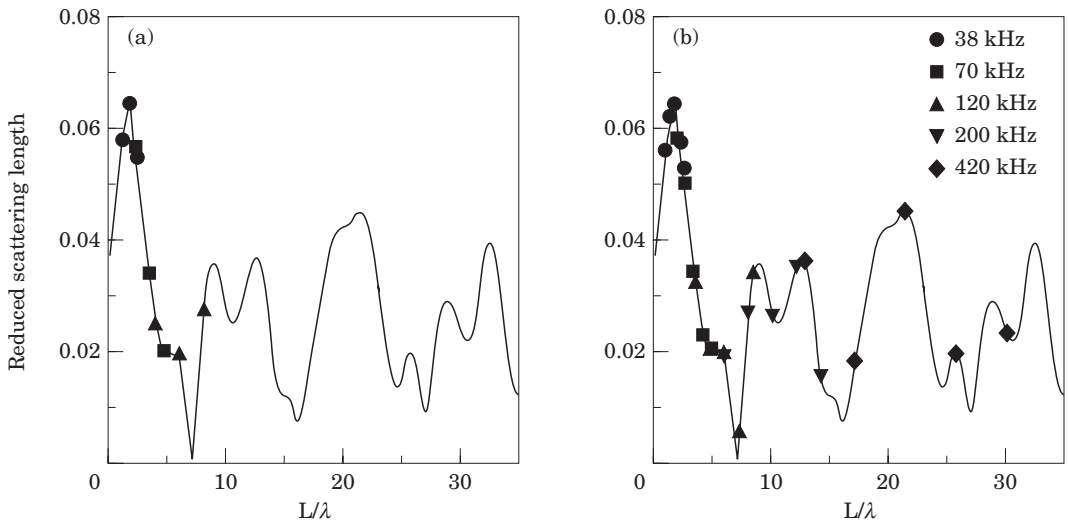


Figure 4. Predicted reduced scattering lengths from the Kirchhoff-ray mode scattering model of threadfin shad (*Dorosoma petenense*) plotted as a function of the ratio of fish length L to acoustic carrier wavelength λ for the unimodal simulated population. (a) Reference points for the scattering matrix formed using the length-class criterion equal intervals centred on the mean length, and carrier frequencies 38, 70, and 120 kHz. (b) Reference points for the scattering matrix formed using the length-class criterion equal intervals centred on the mean length, and carrier frequencies 38, 70, 120, 200, and 420 kHz.

structure is the best way to examine efficacy of the inverse approach. The total number of animals and the length-frequency distributions are not known for populations in natural environments. Modal or mean lengths are easily obtained from net samples, but sample biases due to net selectivity and placement in the water column are not easily determined for natural populations. We calculated total backscatter from the population by summing the backscatter from each individual. Variance in backscatter amplitude due to organism behaviour (e.g. aspect changes), shadowing effects of ensembles, environmental reflectivity (e.g. thermoclines), or violation of stationarity assumptions were not included in calculations.

The use of a single realization of the KRM backscatter model is a second initial condition that potentially influences accuracy of abundance estimates. The scattering curve used in all forward and inverse calculations is based on a single shad. Estimated backscatter amplitudes do not include variability due to allometric or ontogenetic differences among individuals. Variance in backscatter amplitudes may "blur" features along the scattering curve which potentially reduces the amount of information available to discriminate among length classes. This initial condition is consistent with the ideal conditions set for this study but warrants further examination.

We have also exclusively used the non-negative least squares (NNLS) algorithm from Lawson and Hanson (1974) in inverse calculations. We did not use an inverse algorithm that incorporates a smoothing function such as the Bakus–Gilbert algorithm (Backus and Gilbert, 1970) or regularization methods (Phillips, 1962; Tihonov, 1963; Twomey, 1963). A NNLS is recommended as an appropriate, constrained optimization algorithm for both under- and over-determined problems in a variety of aquatic environments (Holliday, 1976; Greenlaw and Johnson, 1983; Holliday and Pieper, 1995).

The influence of organism behaviour potentially introduces a large constraint when inverting backscatter measurements at rather high frequencies (i.e. ka>2, Foote, 1985). Within the geometric scattering region 90% of backscattered sound is reflected from the swimbladder (Foote, 1980), so fish aspect relative to the transducer face is a primary factor in the determination of echo amplitude. In addition, the acoustic contrast at the top surface of the swimbladder is so large that all anatomical structure below the top surface contributes little to the amplitude of backscattered sound (cf. Fig. 8.1.2 Medwin and Clay, 1997). The sensitivity of echo amplitude to aspect angle increases as the ratio of fish length to acoustic wavelength increases. We used the KRM model to estimate threadfin shad echo amplitudes as a function of fish aspect θ, length L, and acoustic carrier frequency λ (Fig. 6). Fish length was set at 75 mm and reduced scattering length (i.e. echo amplitude standardized by fish length) was computed for fish aspects ranging from 60° (head down) to 100° (head up) across the frequency range traditionally used in fisheries acoustic surveys—12 to 420 kHz. Along the fish length to

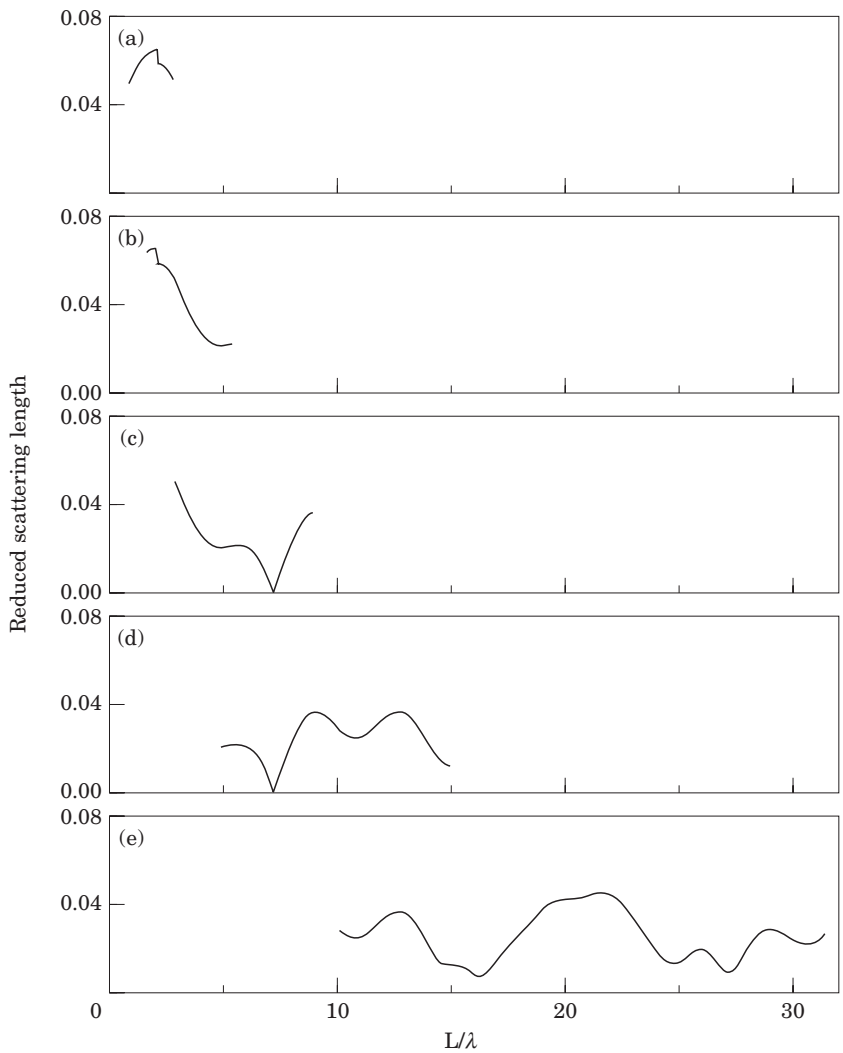


Figure 5. Sections of the threadfin shad (*Dorosoma petenense*) backscatter curve encompassed by each acoustic carrier frequency: (a) 38 kHz; (b) 70 kHz; (c) 120 kHz; (d) 200 kHz; and (e) 420 kHz. Minimum fish length was set at 36 mm and maximum fish length was set at 112 mm in all graphs. The proportions of the total scattering curve increases as frequency increases.

acoustic wavelength axis, if fish length is kept constant then higher L/λ values correspond to higher acoustic frequencies. Keeping the frequency constant illustrates the effect of changes in fish length on echo amplitude. The dependence of echo amplitude on aspect angle at low fish length to acoustic wavelength ratio values. The influence of fish aspect increases as L/λ increases. The response surface becomes quasi-symmetrical as θ deviates positive or negative from 76°. Since maximum backscatter occurs when the top surface of the swimbladder is orthogonal to the transducer face, the threadfin shad swimbladder deviates 14° from the median axis of the fish. The periodic peaks and valleys along the maximum amplitude "ridge" in the surface contour plot correspond to constructive and destructive backscatter interference.

The combination of multiple aspect angles and high L/λ values will introduce variability in backscatter amplitudes. Is this combination likely to occur when using the inverse approach? The inverse approach is applied when multiple frequencies are available and echoes from insonified targets overlap (left side, Fig. 1). Organism behaviour within shoals or schools of fish tends to minimize variability in aspect angles (cf. Shaw, 1970; Okubo, 1986; Huth and Wissel, 1992). Fish tend to swim in coherent, highly polarized aggregations. Among zooplankton, Stanton *et al*. (1993a) has shown that averaging backscatter amplitudes from multiple

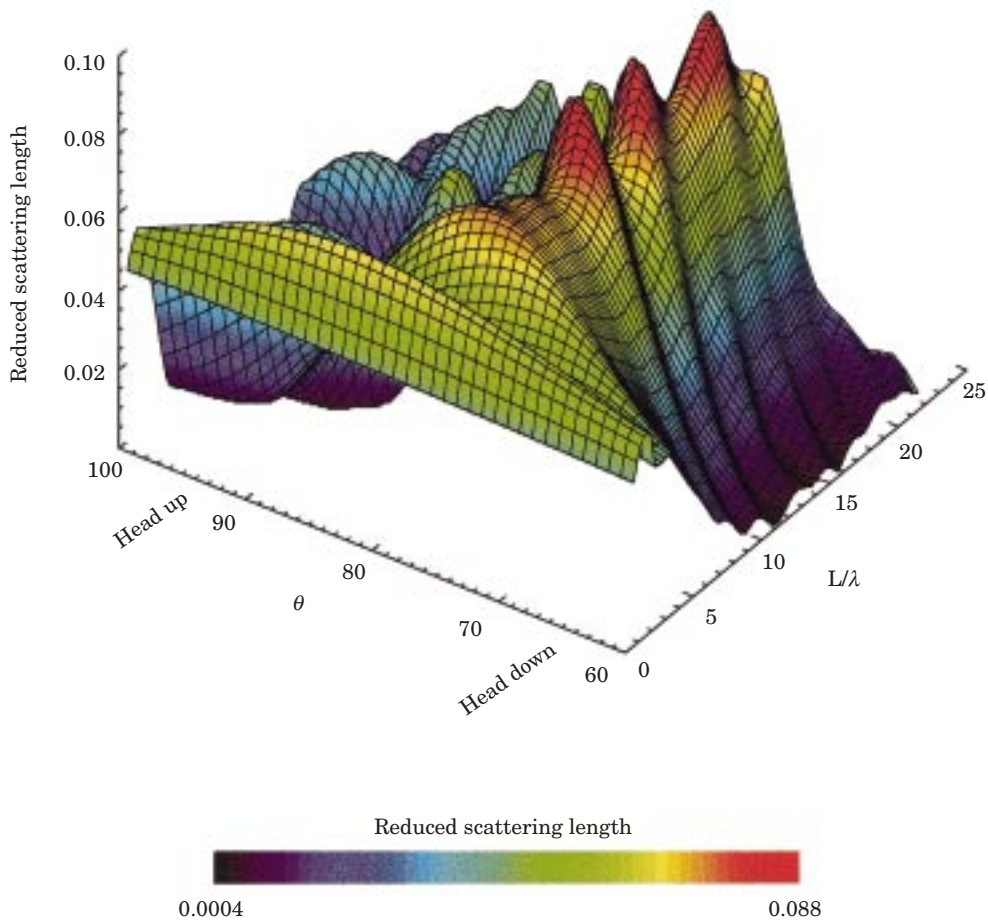


Figure 6. Predicted reduced scattering lengths (i.e. backscatter amplitude standardized by fish length) of threadfin shad (*Dorosoma petenense*) plotted as a function of fish aspect θ and the ratio of fish length L to acoustic frequency wavelength λ. All scattering amplitudes are estimated using the Clay and Horne (1994) Kirchhoff-ray mode backscatter model for a 75 mm fish and a frequency range of 12–420 kHz. Maximum scattering amplitude for any L/λ value occurs at 76°.

individuals tends to reduce amplitude variability in scattering curves. High variability in organism aspect is unlikely to occur within aggregations. If organism aspects deviate from horizontal, possibly during diel vertical migrations, then a constant bias will be introduced in inversion calculations. The amplitude of the bias will be reduced at low L/λ values. Inverse simulations that include aspect variances typically found in the field, and inclusion of low frequency scattering measurements are logical next steps in length-based abundance estimates of fish populations.

Despite the potential constraint of organism aspect, we found that inversion calculations overestimated total abundances by a maximum of 38% and underestimated total abundance by a maximum of 27%. Total abundance deviation index values were consistently low for all frequency and length-class combinations. Within length-class threadfin shad abundance estimates were inconsistent and less accurate than total abundance estimates. Increasing the number of frequencies and length classes used in an inversion simulation did not guarantee more accurate estimates. Future research efforts should focus on determining unique length- and frequency-dependent backscatter characteristics in all scattering regions, refining length-class selection criteria, quantifying accuracy of the inversion method in natural fish populations, incorporating variance in backscatter models due to animal behaviour and morphology, and examining the efficacy of the NNLS algorithm to determine the global minimum error solution.

## Acknowledgements

The authors thank Drs C. Clay, V. Holliday, T. Stanton, P. Wiebe, J. Dalen, and an anonymous reviewer for comments and discussion that improved the manuscript.

D. Deegan and D. Schael provided shad length-frequency data. This work was supported in part by the Office of Naval Research (N00014-1-0989), the Natural Sciences and Engineering Research Council of Canada, and the National Science Foundation (OCE-9415740). This is GLERL contribution #1128.

## References

Anderson, V. C. 1950. Sound scattering from a fluid sphere. Journal of the Acoustical Society of America, 22: 426–431.

Backus, G., and Gilbert, F. 1970. Uniqueness in the inversion of inaccurate gross Earth data. Philosophical Transactions of the Royal Society of London A, 266: 123–197.

Clay, C. S. 1991. Low-resolution acoustic scattering models: Fluid-filled cylinders and fish with swimbladders. Journal of the Acoustical Society of America, 89: 2168–2179.

Clay, C. S. 1992. Composite ray-mode approximations for backscattered sound from gas-filled cylinders and swimbladders. Journal of the Acoustical Society of America, 92: 2173–2180.

Clay, C. S., and Horne, J. K. 1994. Acoustic models of fish: The Atlantic cod (*Gadus morhua*). Journal of the Acoustical Society of America, 96: 1661–1668.

Cochrane, N. A., Sameoto, D., Herman, A. W., and Neilson, J. 1991. Multiple-frequency acoustic backscattering and zooplankton aggregations in the inner Scotian Shelf basins. Canadian Journal of Fisheries and Aquatic Sciences, 48: 340–355.

Dalen, J., and Kristensen, K.-E. 1990. Comparative studies of theoretical and empirical target-strength models of euphausiids (krill) in relation to field-experiment data. Rapports et Proces-Verbaux des Réunions du Conseil International pour l'Exploration de la Mer, 189: 336–344.

Dickie, L. M., Kerr, S. R., and Boudreau, P. R. 1983. An echo counting and logging system (ECOLOG) for demersal fish size distributions and densities. Canadian Journal of Fisheries and Aquatic Sciences, 40: 487–498.

Foote, K. G. 1980. Importance of the swimbladder in acoustic scattering by fish: a comparison of gadoid and mackerel target strengths. Journal of the Acoustical Society of America, 67: 2084–2089.

Foote, K. G. 1985. Rather-high-frequency sound scattered by swimbladdered fish. Journal of the Acoustical Society of America, 78: 688–700.

Foote, K. G. 1987. Fish target strengths for use in echo integrator surveys. Journal of the Acoustical Society of America, 82: 981–987.

Foote, K. G., and Traynor, J. J. 1988. Comparisons of walleye pollock target strength estimates determined from *in situ* measurements and calculations based on swimbladder form. Journal of the Acoustical Society of America, 83: 9–17.

Greenlaw, C. F. 1979. Acoustical estimation of zooplankton populations. Limnology and Oceanography, 24: 226–242.

Greenlaw, C. F., and Johnson, R. K. 1983. Multiple-frequency acoustical estimation. Biological Oceanography, 2: 227–252.

Hasslett, R. W. G. 1969. The target strengths of fish. Journal of Sound Vibration, 9: 181–191.

Holliday, D. V. 1972. Resonance structure in echoes from schooled pelagic fish. Journal of the Acoustical Society of America, 51: 1322–1332.

Holliday, D. V. 1976. Technical report on exploratory development in the application of swimbladder resonance techniques to marine surveys. TRACOR Document No. T-76-SD-1101-U, 54 pp. (Tracor Applied Sciences, 9150 Chesapeake Drive, San Diego, CA 92123-1003).

Holliday, D. V. 1977. Extracting bio-physical information from the acoustic signatures of marine organisms. *In* Oceanic sound scattering prediction, pp. 619–624. Ed. by N. R. Andersen, and B. J. Zahuranec. Plenum, New York.

Holliday, D. V. 1980. Use of acoustic frequency diversity for marine biological measurements. *In* Advanced Concepts in Ocean Measurements for Marine Biology, pp. 423–460. Ed. by F. P. Diemer. The Belle W. Raruch Library in Marine Science, Number 10.

Holliday, D. V., and Pieper, R. E. 1995. Bioacoustical oceanography at high frequencies. ICES Journal of marine Science, 52: 279–296.

Holliday, D. V., Pieper, R. E., and Kleppel, G. S. 1989. Determination of zooplankton size and distribution with multifrequency acoustic technology. Journal du Conseil International pour l'Exploration de la Mer, 46: 52–61.

Horne, J. K., and Clay, C. S. 1998. Sonar systems and aquatic organisms: matching equipment and model parameters. Canadian Journal of Fisheries and Aquatic Sciences, 55: 1296–1306.

Huth, A., and Wissel, C. 1992. The simulation of the movement of fish schools. Journal of Theoretical Biology, 156: 365–385.

Jech, J. M., Schael, D. M., and Clay, C. S. 1995. Application of three sound scattering models to threadfin shad (*Dorosoma petenense*). Journal of the Acoustical Society of America, 98: 2262–2269.

Johnson, R. K. 1977a. Sound scattering from a fluid sphere revisited. Journal of the Acoustical Society of America, 62: 375–377.

Johnson, R. K. 1977b. Acoustic estimation of scattering-layer composition. Journal of the Acoustical Society of America, 61: 1636–1639.

Kalish, J. M., Greenlaw, C. F., Pearcy, W. G., and Holliday, D. V. 1986. The biological and acoustical structure of sound scattering layers off Oregon. Deep-Sea Research, 33: 631–653.

Kleppel, G. S., Frazel, D., Pieper, R. E., and Holliday, D. V. 1988. Natural diets of zooplankton off southern California. Marine Ecology Progress Series, 49: 231–241.

Lawson, C. L., and Hanson, R. J. 1974. Solving least squares problems. Prentice-Hall, Englewood Cliffs.

Love, R. H. 1977. Target strength of an individual fish at any aspect. Journal of the Acoustical Society of America, 62: 1397–1403.

McNaught, D. C. 1968. Acoustical determination of zooplankton distributions. Proceedings of the 11th Conference on Great Lakes Research, 1968: 76–84.

McNaught, D. C. 1969. Developments in acoustic plankton sampling. Proceedings of the 12th Conference on Great Lakes Research 1969: 61–68.

Medwin, H., and Clay, C. S. 1997. Applied Ocean Acoustics: Fundamentals of Acoustical Oceanography. Academic Press, New York.

Megrey, B. A. 1989. Review and comparison of age-structured stock assessment models from theoretical and applied points of view. American Fisheries Society Symposium, 6: 8–48.

Napp, J. M., Ortner, P. B., Pieper, R. E., and Holliday, D. V. 1993. Biovolume-size spectra of epipelagic zooplankton using a Multifrequency Acoustic Profiling System (MAPS). Deep-Sea Research, 40: 445–459.

Nero, R. W., Thompson, C. H., and Love, R. H. 1997. Abyssopelagic grenadiers – the probable cause of low frequency sound scattering at great depths off the Oregon and California coasts. Deep-Sea Research, 44: 627–645.

Okubo, A. 1986. Dynamical aspects of animal grouping, swarms, schools, flocks, and herds. Advances in Biophysics, 22: 1–94.
Penrose, J. D., and Kaye, G. T. 1979. Acoustic target strengths of marine organisms. Journal of the Acoustical Society of America, 65: 374–380.
Phillips, D. L. 1962. A technique for the numerical solution of certain integrals of the first kind. Journal of the Association for Computing Machinery, 9: 84–97.
Pieper, R. E., Holliday, D. V., and Kleppel, G. S. 1990. Quantitative zooplankton distributions from multifrequency acoustics. Journal of Plankton Research, 12: 433–441.
Sætersdal, G., Stromme, T., Bakken, B., and Piekutowski, L. 1984. Some observations on frequency-dependent backscattering strength. FAO Fisheries Reports, 300: 150–156.
Schael, D. M. 1993. Spatial and temporal distribution of Threadfin Shad (*Dorosoma petenense*) in a multipurpose reservoir. M.Sc. thesis, North Carolina State University.
Shaw, E. 1970. Schooling in fishes: critique and review. *In* Development and Evolution of Behaviour, pp. 452–480. Ed. by L. Aronson. Freeman, San Francisco.
Simmonds, E. J., Williamson, N. J., Geroltto, F., and Aglen, S. 1988. Acoustic survey design and analysis procedure: a comprehensive review of current practice. ICES Cooperative Research Report, No. 187, 131 pp.
Smith, S. L., Pieper, R. E., Moore, M. V., Rudstam, L. G., Greene, C. H., Zamon, J. E., Flagg, C. N., and Williamson, D. E. 1992. Acoustic techniques for the *in situ* observation of zooplankton. Archiv für Hydrobioloie Beiheft Ergebnisse der Limnologie, 36: 23–43.
Sparre, P., Ursin, E., and Venema, S. C. 1989). Introduction to tropical fish stock assessment. Part 1. Manual. FAO Fisheries Technical Paper. No. 306.1. Rome, 337 pp.
Stanton, T. K. 1988. Sound scattering by cylinders of finite length I. Fluid cylinders. Journal of the Acoustical Society of America, 83: 55–63.
Stanton, T. K. 1989. Sound scattering by cylinders of finite length. III. Deformed cylinders. Journal of the Acoustical Society of America, 86: 691–705.
Stanton, T. K., Chu, D., Wiebe, P. H., and Clay, C. S. 1993a. Average echoes from randomly oriented random-length finite cylinders: zooplankton models. Journal of the Acoustical Society of America, 94: 3463–3472.
Stanton, T. K., Clay, C. S., and Chu, D. 1993b. Ray representation of sound scattering by weakly scattering deformed fluid cylinders: simple physics and application to zooplankton. Journal of the Acoustical Society of America, 94: 3453–3462.
Thompson, C. H., and Love, R. H. 1996. Determination of fish size distributions and areal densities using broadband low-frequency measurements. ICES Journal of marine Science, 53: 197–201.
Tihonov, A. H. 1963. Regularization of incorrectly posed problems. Soviet Mathematics-Doklady, 4: 1624–1627.
Twomey, S. 1963. On the numerical solution of Fredholm integral equations of the first kind by the inversion of a linear system produced by quadrature. Journal of the Association for Computing Machinery, 10: 97–101.
Williamson, N. J., and Traynor, J. J. 1984. *In situ* target strength estimation of Pacific whiting (*Merluccius productus*) using a dual-beam transducer. Journal du Conseil International pour l'Exploration de la Mer, 41: 285–292.
Ye, Z. 1997. A novel approach to sound scattering by cylinders of finite length. Journal of the Acoustical Society of America, 102: 877–884.
Ye, Z., Hoskinson, E., Dewey, R. K., Ding, L., and Farmer, D. M. 1997. A method for acoustic scattering by slender bodies. I. Theory and verification. Journal of the Acoustical Society of America, 102: 1964–1976.
Zakharia, M., and Sessarego, J. P. 1982. Sonar target classification using a coherent echo processing. *In* Proceedings of the IEEE International Conference on Acoustics, Speech, and Signal Processing, pp. 331–334. IEEE, Paris.

# Appendix A: Kirchhoff Ray-mode Model

Foote (1985) and Foote and Traynor (1988) used the Helmholtz-Kirchhoff integral to develop an accurate and elaborate method to estimate backscatter from fish. Clay and Horne (1994) simplified the approach in the Kirchhoff-ray mode (KRM) backscatter model by modelling the fish body and swimbladder as a set of fluid and gas filled cylinders. The KRM model was verified by Jech *et al.* (1995) who compared predicted backscatter from threadfin shad (*Dorsoma petenense*) to controlled measures at 120, 200, and 420 kHz. Using digitized images of the fish swimbladder and body, the KRM model estimates backscatter using a low mode cylinder solution and a Kirchhoff-ray approximation. The morphology of the fish swimbladder and body, obtained by dissection or x-rays, is used to construct finite cylinders (Fig. A1a) and then transformed from x–z Cartesian coordinates to u–v coordinates relative to the incident wavefront (Fig. A1b). Backscattering cross-sections from each finite cylinder are summed over the whole swimbladder or body and then added coherently.

For the swimbladder only and ka<0.2, a low mode (M=0) cylinder solution is used (Clay, 1991, 1992). The finite bent cylinder equation from Stanton (1989) is modified, where the roughness coefficient is eliminated, the phase shift is replaced with the geometry of the swimbladder, and scattering is calculated for backscatter only (i.e. the wavefront is in dorsal aspect). We write the summation of the backscatter for $N_e$ cylinders as:

$$\mathscr{L}(f) = \frac{-i}{\pi} \sum_{j}^{N_e} b_0 e^{-i2kv(j)} dx(j) \tag{A1}$$

$$b_0 = \frac{-1}{1 + iC_0},$$

$$C_0 = \frac{J_0'(k_1a)N_0(ka) - ghN_0'(ka)J_0(k_1a)}{J_0'(k_1a)J_0(ka) - ghJ_0'(ka)J_0(k_1a)},$$

$$g = \frac{\rho_1}{\rho_w}, \quad h = \frac{c_1}{c_w}$$

where $\mathscr{L}(f)$ is the scattering amplitude as a function of carrier frequency, ρ is density, c is sound speed, k is the wavenumber ($2\pi/\lambda$), λ is the acoustic wavelength, J is the cylindrical Bessel function of the first kind of order 0, N is the cylindrical Bessel function of the second kind of order 0, J′ and N′ are derivatives of J and N, the

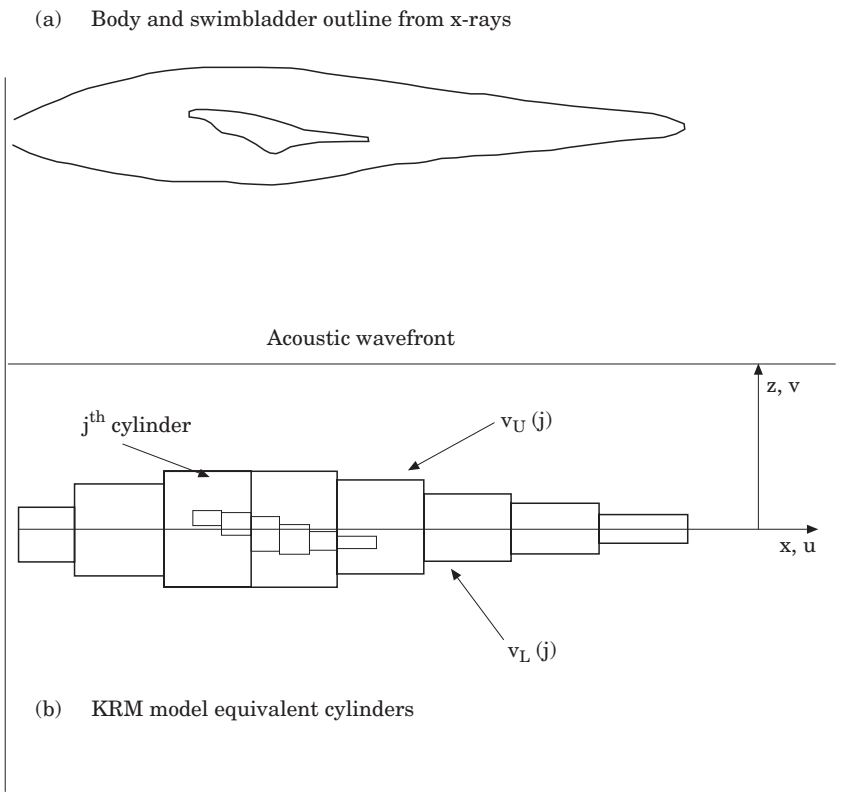


Figure A1. (a) Fish body and swimbladder outline from lateral x-ray. (b) Kirchhoff-ray mode model representation of fish body and swimbladder. The body is represented by a set of fluid-filled cylinders and the swimbladder is represented by a set of gas-filled cylinders. The Cartesian x–y coordinate system is transformed to a u–v fish centred coordinate system.

subscripts "l" and "w" denote cylinder and water respectively, a is the cylinder radius, and dx(j) represents the incremental distance between the midpoint of each ($j^{th}$) cylinders.

For the swimbladder and ka>0.2, a Kirchhoff-ray approximation is used. Equation (11) in Clay (1992) is modified to sum the backscatter from $N_e$ swimbladder elements:

$$\mathscr{L}(f) = -i\frac{R_{fs}(1-R_{wf}^2)}{2\sqrt{\pi}} \sum_{j=0}^{N_e-1} A_{sb}[k_{fb}a(j) + 1]^{1/2} e^{-i[2k_{fb}v_u(j)+\Psi_{sb}]}\Delta u(j) \quad \text{(A2)}$$

$$A_{sb} = \frac{ka(j)}{ka(j)+0.083}, \quad \Psi_{sb} = \frac{ka(j)}{[40+ka(j)]} - 1.05,$$

$$R_{fs} = \frac{g'h'-1}{g'h'+1}, \quad R_{wf} = \frac{\rho_{fb}c_{fb}-\rho_w c_w}{\rho_{fb}c_{fb}+\rho_w c_w},$$

$$g' = \frac{\rho_{sb}}{\rho_{fb}}, \quad h' = \frac{c_{sb}}{c_{fb}}$$

A similar expression is derived for the fish body:

$$\mathscr{L}(f) = -i\frac{R_{wf}}{2\sqrt{\pi}} \sum_{j=0}^{N_e-1} [ka(j)]^{1/2}[e^{-i2kv_u(j)} - (1-R_{wf}^2) \times e^{i(-2kv_u(j)+2k_{fb}(v_u(j)-v_L(j)+\Psi_{fb}))}]\Delta u(j), \quad \text{(A3)}$$

$$\Psi_{sb} = -\frac{\pi k_{fb} v_U(j)}{2[k_{fb}v_U(j)+0.4]}, \; k_{sb} = \frac{2\pi f}{c_{fb}}$$

where R is the reflection coefficient, subscript wf denotes the water-fish body interface, fs denotes the swimbladder-fish body interface, fb refers to the fish body, sb refers to the swimbladder, and U and L refer to the upper and lower surfaces in u–v coordinates, respectively. Δu(j) denotes incremental distance between cylinders. $A_{sb}$ and $\Psi_{sb}$ are empirical amplitude and phase adjustments for small ka.

The backscattering cross-section ($\sigma_{bs}$) is computed from the complex scattering length $\mathscr{L}(f)$ for all three models by:

$$\sigma_{bs}(f) = |\mathscr{L}(f)|^2 \quad \text{(A4)}$$

Reduced scattering length is:

$$\text{reduced scattering length} = \frac{|\mathscr{L}(f)|}{TL} \tag{A5}$$

Reduced $\sigma_{bs}$ is:

$$\text{reduced } \sigma_{bs} = \frac{|\mathscr{L}(f)|^2}{TL^2} \tag{A6}$$

and the reduced target strength (TS) is:

$$\text{reduced TS} = 20 \log_{10}\left[\frac{\mathscr{L}(f)}{TL}\right] \tag{A7}$$

The scattering lengths for the fish body and swimbladder were computed individually. Whole fish scatter [$\mathscr{L}_{wf}(f)$] can be computed from the fish body [$\mathscr{L}_{fb}(f)$] and swimbladder [$\mathscr{L}_{sb}(f)$]. Coherent scatter is assumed and thus $\mathscr{L}_{fb}(f)$ and $\mathscr{L}_{sb}(f)$ add as the complex functions:

$$\mathscr{L}_{wf}(f) = \mathscr{L}_{fb}(f) + \mathscr{L}_{sb}(f) \tag{A8}$$

Values for equivalent cylindrical parameters and physical variables used in the backscatter models are given in Jech *et al*. (1995).